Anal. Chem. **2006,** *78,* 3084−3089

Microfluidic Single-Cell mRNA Isolation and Analysis

Joshua S. Marcus,[†,‡] W. French Anderson,[‡,§] and Stephen R. Quake*[,‡,||]

Biochemistry and Molecular Biophysics, and Applied Physics and Physics, California Institute of Technology, MS 128-95, Pasadena, California 91125, and Gene Therapy Laboratories, Keck School of Medicine, University of Southern California, Los Angeles, California 90033

Single-cell gene expression analysis holds great promise for studying diverse biological systems, but methodology to process these precious samples in a reproducible, quantitative, and parallel fashion remains challenging. Here, we utilize microfluidics to isolate picogram and subpicogram mRNA templates, as well as to synthesize cDNA from these templates. We demonstrate single-cell mRNA isolation and cDNA synthesis, provide quantitative calibrations for each step in the process, and measure gene expression in individual cells. The techniques presented here form the foundation for highly parallel single-cell gene expression studies.

It is in general challenging to study mRNA levels in single cells. Techniques that are commonplace for population studies, such as differential display, subtractive cloning, and serial analysis of gene expression, are not yet amenable to the study of individual cells.[1] Currently, the most widely used assay for obtaining information about specific gene expression levels is cDNA synthesis from a cellular mRNA template using the RNA-dependent DNA polymerase reverse transcriptase (RT) coupled to the polymerase chain reaction (PCR).[2] This technique, analyzed either with end point gel electrophoresis or with real-time fluorescence, has in a few instances, been applied to single cells.[3−7] Probing specific gene expression with fluorescence in situ hybridization has also been accomplished in fixed cells by utilizing computational fluorescence microscopy.[8] A few groups have applied RT-PCR and T7 mRNA amplification approaches to prepare cDNA for single-cell microarray analysis.[9−12] Although these researchers were able to ask questions about global gene expression in single cells, each group was limited in their ability to process a large number of cells. For example, in one study,[12] 90 cells were isolated by laser capture microdissection, but only 16 exhibited robust expression of the ubiquitous transcript glyceraldehyde-3-phosphate dehydrogenase (GAPDH). Single-cell cDNA library construction has been utilized sparingly and is limited to medium- and high-abundance transcripts.[13−16]

The paucity of single-cell RT-PCR studies has been attributed to the laborious and difficult task of purifying mRNA from individual cells and subsequently synthesizing and purifying total single-cell cDNA.[17] The difficulty is due to the loss of material during the subsequent steps of cell isolation, lysis, mRNA isolation, and cDNA synthesis. Reasons for the loss include mRNA degradation due to RNases or damage, nonspecific adhesion to the reaction vessel, and reverse transcription not going to completion.

Because of the small reaction volumes and the ability for automation, microfluidic devices are the ideal platform to analyze single cells in a high-throughput, highly parallel fashion. Previous work in our laboratory demonstrated the feasibility of using microfluidic devices with integrated micromechanical valves to isolate mRNA and genomic DNA from small numbers of mammalian and bacterial cells, respectively.[18] In this report, we implement a more robust isolation and purification scheme, provide the first quantitative calibrations for microfluidic mRNA isolation and cDNA synthesis, and demonstrate sensitivity sufficient to detect medium and low copy number transcripts in single cells. All five steps (cell capture, cell lysis, mRNA purification, cDNA synthesis, cDNA purification) were implemented in a microfluidic assay on one integrated device.

* To whom correspondence should be addressed. E-mail: quake@stanford.edu.
† Biochemistry and Molecular Biophysics, California Institute of Technology.
‡ Applied Physics and Physics, California Institute of Technology.
§ University of Southern California.
|| Current address: Bioengineering Department, Stanford University, Clark Center E350Q, Stanford, CA 94305.

(1) Li, B. *Electron. J. Biotechnol.* **2005**, *8*, 71−81.
(2) Bustin, S. A. *J. Mol. Endocrinol.* **2000**, *25*, 169−193.
(3) Bengtsson, M.; Stahlberg, A.; Rorsman, P.; Kubista, M. *Genome Res.* **2005**, *15*, 1388−1392.
(4) Danik, M.; Puma, C.; Quirion, R.; Williams, S. *J. Neurosci. Res.* **2003**, *74*, 286−295.
(5) Henne, J.; Pottering, S.; Jeserich, G. *J. Neurosci. Res.* **2000**, *62*, 629−637.
(6) Lindqvist, N.; Vidal-Sanz, M.; Hallbook, F. *Brain Res. Brain Res. Protoc.* **2002**, *10*, 75−83.
(7) Peixoto, A.; Monteiro, M.; Rocha, B.; Veiga-Fernandes, H. *Genome Res.* **2004**, *14*, 1938−1947.
(8) Levsky, J. M.; Shenoy, S. M.; Pezo, R. C.; Singer, R. H. *Science* **2002**, *297*, 836−840.
(9) Chiang, M. K.; Melton, D. A. *Dev. Cell* **2003**, *4*, 383−393.
(10) Kamme, F.; Salunga, R.; Yu, J.; Tran, D. T.; Zhu, J.; Luo, L.; Bittner, A.; Guo, H. Q.; Miller, N.; Wan, J.; Erlander, M. *J. Neurosci.* **2003**, *23*, 3607−3615.
(11) Luo, L.; Salunga, R. C.; Guo, H.; Bittner, A.; Joy, K. C.; Galindo, J. E.; Xiao, H.; Rogers, K. E.; Wan, J. S.; Jackson, M. R.; Erlander, M. G. *Nat. Med.* **1999**, *5*, 117−122.
(12) Tietjen, I.; Rihel, J. M.; Cao, Y.; Koentges, G.; Zakhary, L.; Dulac, C. *Neuron* **2003**, *38*, 161−175.
(13) Bishop, J. O.; Morton, J. G.; Rosbash, M.; Richardson, M. *Nature* **1974**, *250*, 199−204.
(14) Dulac, C.; Axel, R. *Cell* **1995**, *83*, 195−206.
(15) Matsunami, H.; Buck, L. B. *Cell* **1997**, *90*, 775−784.
(16) Pantages, E.; Dulac, C. *Neuron* **2000**, *28*, 835−845.
(17) Liss, B. *Nucleic Acids Res.* **2002**, *30*, e89.
(18) Hong, J. W.; Studer, V.; Hang, G.; Anderson, W. F.; Quake, S. R. *Nat. Biotechnol.* **2004**, *22*, 435−439.

10.1021/ac0519460 CCC: $33.50
Published on Web 03/31/2006

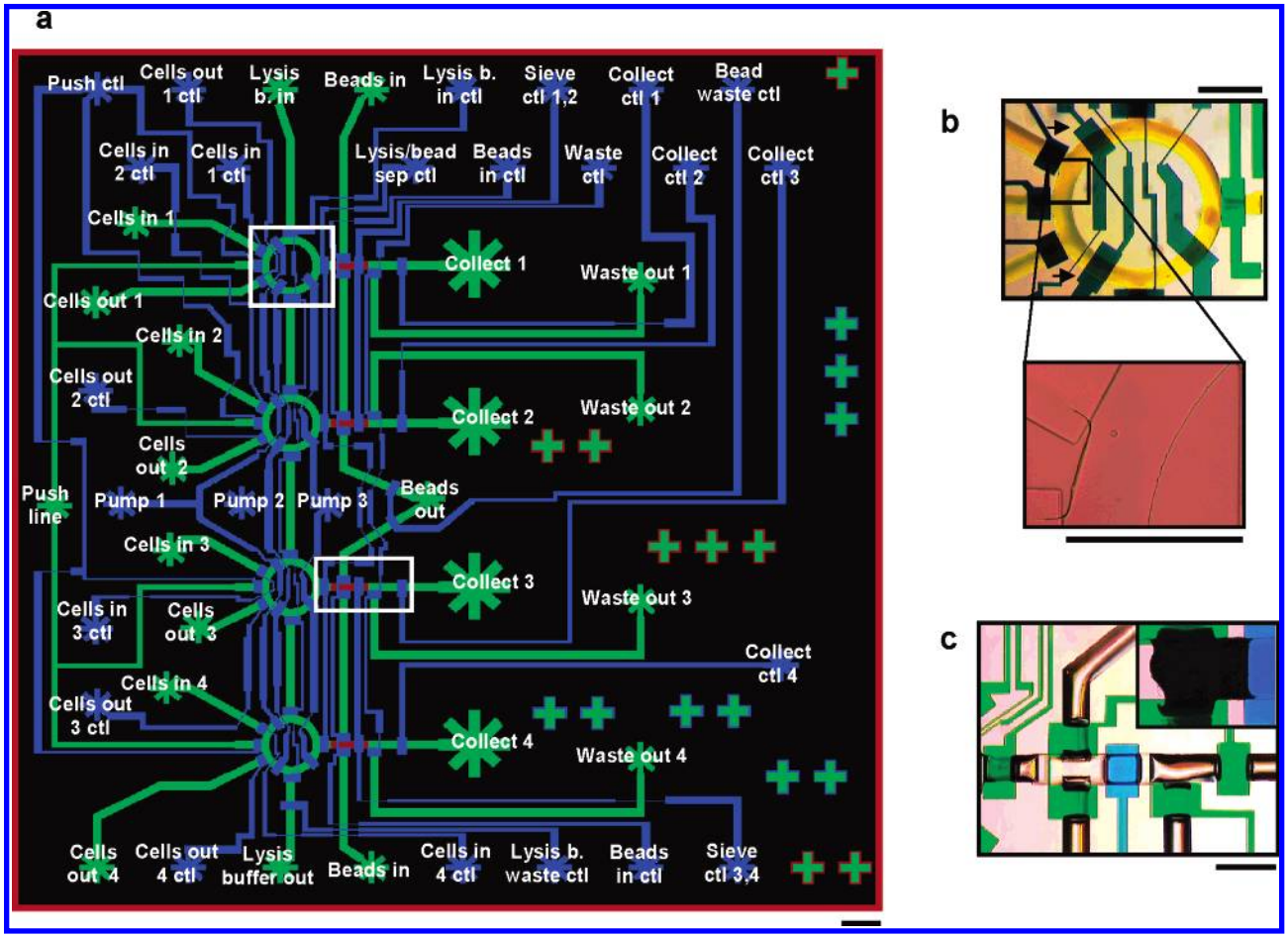

Figure 1. 4plex mRNA isolation/first strand synthesis device. (a) AutoCAD drawing of a device with inputs and outputs labeled according to function. Rounded flow channels are depicted in green and control channels are shown in blue. Unrounded (rectangular profile) flow channels for affinity column construction are shown in red. Portions of drawing in white boxes are shown in (b) and (c), respectively. (b) Optical micrographs of the lysis ring and an NIH/3T3 cell captured in the ring. (c) Optical micrographs of the affinity column construction area and a stacked column. Scale bars are 400 μm.

EXPERIMENTAL SECTION

Device Fabrication. All devices were fabricated using the process of multilayer soft lithography.[19] Devices are composed of three layers of the silicone elastomer poly(dimethylsiloxane) (General Electric) bonded to a RCA cleaned No. 1.5 glass coverslip and were fabricated as previously described,[20] but with slight modifications.[21] Negative master molds were fabricated out of photoresist by standard optical lithography and patterned with 20 000 dpi transparency masks (CAD/Art Services) drafted with AutoCAD software (Autodesk). The flow layer masks were sized to 101.5% of the control layer masks to compensate for shrinking of features during the first elastomer curing step. The flow master molds were fabricated out of 40-μm AZ-100XT/13-μm SU8-2015 photoresists (Clariant/Microchem), and the control molds were cast from 24-μm SU8-2025 (Microchem). The procedures for master mold and device fabrication are described in detail in the Supporting Information.

General Device Operation. The on−off valves within each device are controlled by individual pressure sources (Fluidigm) and are interfaced via 23-gauge pins (New England Small Tube) and Tygon tubing (VWR). A NI-DAQ card and Labview interface (National Instruments) were used to actuate the pressure sources.

Reagent Preparation. Lysis and wash buffers are brought to room temperature before utilization. Paramagnetic beads derivatized with oligo(dT)$_{25}$ sequences (Dynal Biotech) are suspended in lysis buffer to 3× the manufacturer's concentration. The first strand synthesis reaction is prepared according to the manufacturer's protocol (Qiagen), with enzymes left out until the reaction is ready to be performed on-chip. PCR collection buffer is prepared by bringing the respective PCR buffer to 1× concentration in H_2O.

Microfluidic mRNA Isolation and cDNA Synthesis Process Flow. Nucleic acid processing was performed in one of two ways: single reactions in a serial manner or four reactions in parallel with the 4plex device. An autoCAD drawing of a 4plex device, as well as optical micrographs of sections of a device are pictured in Figure 1. The devices contain modules for (1) cell lysis (Figure 1b), (2) mRNA isolation/cDNA synthesis/purification (Figure 1c), and (3) product collection. We performed single isolations serially for initial proof-of-principle studies, utilizing gel electrophoresis for analysis. The samples processed in parallel were analyzed with qPCR.

Lysis buffer is loaded into all flow lines in the device through the specified inlet (Figure 1a), except for the lines utilized for

(19) Unger, M. A.; Chou, H. P.; Thorsen, T.; Scherer, A.; Quake, S. R. *Science* **2000**, *288*, 113−116.
(20) Fu, A. Y.; Spence, C.; Scherer, A.; Arnold, F. H.; Quake, S. R. *Nat. Biotechnol.* **1999**, *17*, 1109−1111.
(21) Studer, V. H., G.; Pandolfi, A.; Ortiz, M.; Anderson, W. F.; Quake, S. R. *J. Appl. Phys.* **2004**, *95*, 393−398.

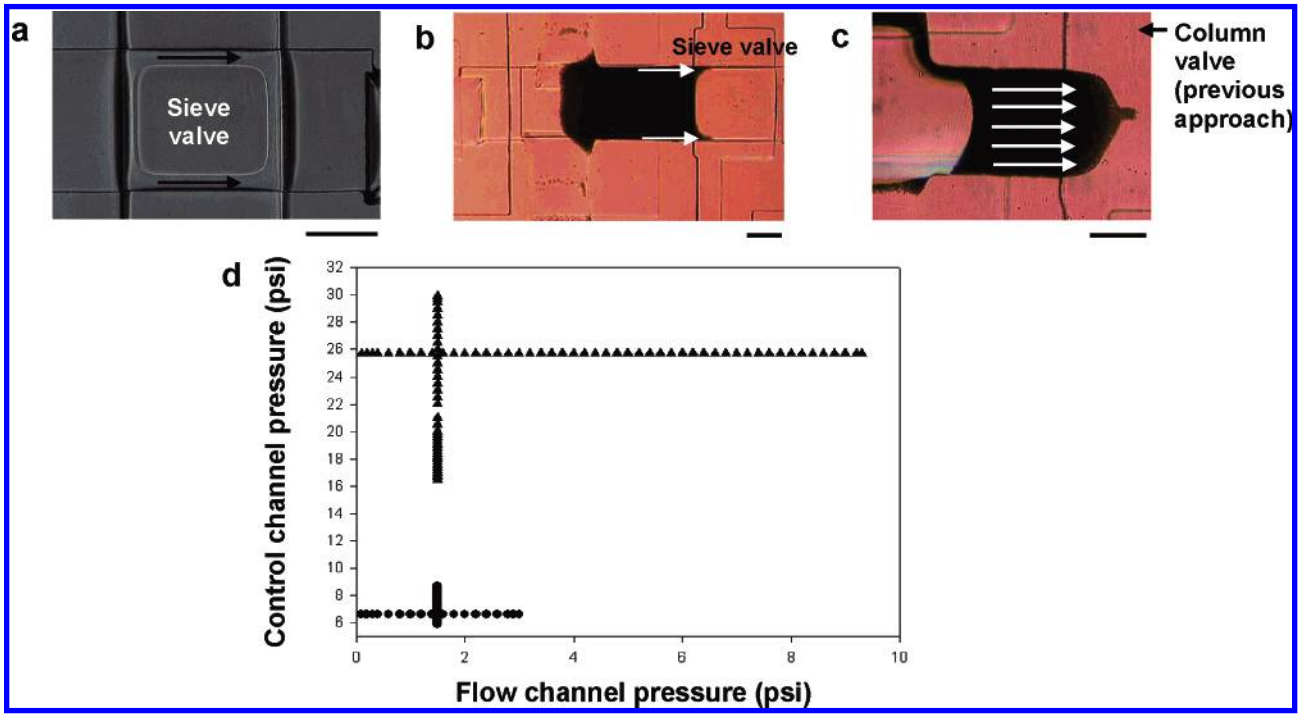

Figure 2. Microfluidic sieve valve. (a) Top-down image of an actuated sieve valve. (b) Optical micrograph of a stacked column using a sieve valve. Arrows indicate where beads have the capacity to escape. (c) Optical micrograph of a stacked column utilizing the previous approach. Arrows indicate where beads have the potential to escape. Scale bars are 100 μm. (d) Sampling of parameter space sufficient to build functional bead columns. Triangles represent the sieve valve method, and circles represent the previous approach.[18] The flow channel pressure is the pressure applied to the bead inlet and the column pressure is the pressure applied to the column valve's inlet.

cell loading and capture. This is accomplished by keeping pump valves 1 and 2 closed (Figure 1a). The beads are then loaded onto the chip in a north−south south−north fashion (Figure 1a), depending on which reactor is used, and subsequently stacked against sieve valves (Figures 1c and 2).[22] When loading the beads, the waste valves are open and the collection and lysis ring/bead separation control channels are closed, so as not to contaminate other areas of the device with beads (Figure 1a, c).

Sieve valves are present on a portion of a 200-μm-wide, 10-μm-high flow channel with a rectangular profile. A top-down view of a closed sieve valve (Figure 2a, b) shows when the valve is actuated, flow is restricted to the top and bottom ~10 μm of the channel. Previous microfluidic column designs in our group used a slightly opened valve present on a flow channel with a semicircular profile to allow fluid flow, while not allowing beads to pass (Figure 2c).[18] A sampling of parameter space sufficient to build functional bead columns by the two methods is given in Figure 2d. We either applied 1.5 psi pneumatic pressure to the bead inlet while varying the column valve's pressure or kept the column valve's pressure constant while varying the pressure applied to the flow inlet. Using the sieve approach, flow pressure can be varied by 1 order of magnitude more than the first-generation column, measured by whether the beads escape to waste (Figure 2d). Similarly, when applying constant pressure to the bead inlet, the pressure applied to the sieve valve used to stack the beads can be adjusted 7-fold more than its first-generation counterpart. Because of the sieve valve's functionality over a breadth of parameter space, it enables columns to be constructed in a digital manner. This is contrasted to its analog predecessor,[18] where pressures needed to be finely tuned in order to obtain a functional column. The digital and analog nature of the respective columns is evident when visualizing the flow profile through stacked columns, and where in the channel beads can potentially escape (arrows in Figure 2a and b). If the applied flow pressure over a column built by the previous method becomes too great, beads can escape at any point in the channel, whereas beads can only escape at the top and bottom portions (top-down view) of the channel if a column is built against a sieve valve.

After affinity column construction, NIH/3T3 cells or purified NIH/3T3 mRNA (Ambion) are loaded into a 4-nL portion of the lysis ring between the valves for pumps 1 and 2 (Figure 1a, b). The contents of the ring are subsequently mixed[23,24] and pressure-driven over the affinity columns. Once mRNA capture is complete, a wash step is implemented. Then, the bead−mRNA complexes are collected by opening the sieve valve, closing the waste lines, and sending the beads to the output ports in RT-PCR buffer. Alternatively, solid-phase cDNA synthesis is performed directly on the affinity columns. To do this, the columns are flushed with RT and dNTPs in a first strand reaction buffer for 45 min, followed by heating the chips to 40°C on a thermal microscope stage to activate the polymerase. The dT sequences on the beads are used as primers. When cDNA synthesis is complete, the bead−cDNA complexes are sent to the output ports in PCR buffer, collected with gel loading tips (Promega), and frozen, pending future analysis.

(22) Sieve valve designed in collaboration with Carl Hansen.

(23) Chou, H. P.; Unger, M. A.; Quake, S. R. *Biomed. Microdevices* **2001**, *3*, 323−330.
(24) Hansen, C. L.; Sommer, M. O.; Quake, S. R. *Proc. Natl. Acad. Sci. U S A* **2004**, *101*, 14431−14436.

NIH/3T3 Cell Preparation. NIH/3T3 cells were grown to ~70% confluency in Dulbecco's modified Eagle medium/10% calf serum (Hyclone) in 12.5-cm^2 vacuum-gas plasma-treated polystyrene culture flasks (BD Falcon). Cells were then washed in 1× PBS, trypsinized, and further diluted in culture medium to stop the trypsinization reaction. After counting the cells, the cell suspension was washed in 1× PBS. The cells in the suspension were then pelleted at 2040*g* for 5 min and suspended in 1× PBS to a concentration of 10^6 cells/mL.

Conventional and Real-Time qPCR. A 132-bp portion of GAPDH was amplified from either the mRNA or 1st strand cDNA template using the following primers: GAPDH sense 5′-CCTGGAGAAACCTGCCAAGTATG-3′; GAPDH antisense 5′-AGAGTGGGAGTTGCTTTGAAGTC-3′.

A 294-bp portion of HPRT was amplified with the following primers: hypoxanthine phosphoribosyl transferase (HPRT) sense 5′-GCTGGTGAAAAGGACCTCT-3′; HPRT antisense 5′-CACAGGACTAGAACAACCTGC-3′.

For real-time qPCR cycling, SYBR green was used as a probe in a Roche Lightcycler 1.5 according to the following thermal cycling protocol: 95 °C for 15 min and 35 cycles of 94 °C for 15 s, 55 °C for 20 s, and 72 °C for 15 s. Detection was enabled at 79 °C for GAPDH and 72 °C for HPRT. Postrun melt curve analysis confirmed all products formed were full length and not primer dimers.

Conventional thermal cycling was carried out according to the following protocol: 95 °C for 15 min and 30 cycles of 94 °C for 30 s, 56 °C for 1 min, and 72 °C for 1 min, followed by a final extension phase at 72 °C for 10 min. PCR products were visualized by SYBR green fluorescence on 1% agarose gels.

RESULTS AND DISCUSSION

Microfluidic mRNA Isolation. We first studied the efficiency and reproducibility of the microfluidic mRNA affinity purification step with purified mRNA from NIH/3T3 cells. These samples were loaded onto the chip shown in Figure 1, captured on bead columns, followed by product−bead recovery and analysis with benchtop RT-qPCR. We measured the medium-abundance mRNA GAPDH (~1800 copies/cell, Figure S-1a, Supporting Information) and the low copy number mRNA HPRT (5−10 copies/cell[25]). For the two linear regression lines fitted to the threshold cycles (Ct) of the on-chip standards, R values of 0.98−0.99 were obtained (Figure S-1b). The measured sensitivity and dynamic range for GAPDH probed samples are 0.3−100 pg of NIH/3T3 mRNA, suitable for assays on 1−100 cells (Figure 3). We achieved an average isolation/recovery efficiency of 80% for the samples interrogated for GAPDH (Figure 3). For the purposes of this discussion, 100% efficiency is defined as what one achieves from an RT-qPCR utilizing purified templates subjected to no isolation procedure (e.g., a benchtop standard curve with defined mRNA standards). We were also able to detect HPRT from NIH/3T3 mRNA templates ranging from 1 to 100 pg, both on- and off-chip (Figure S-1b, c), but observed that the amplification efficiency for the on-chip samples differed from that of the off-chip samples. This complicates efforts[26] to calculate a reliable isolation/recovery efficiency using HPRT as a marker. At this point, we are only able to determine relative amounts of HPRT in a sample, without absolute quantification. The coefficient of deviation (experimental noise) for the GAPDH efficiency measurements was 14%. This noise can be attributed mainly to pipetting error in the downstream qRT-PCR reaction setups, different reagent lots for the on- and off-chip standard curve experiments, and loss of product during recovery from the devices.

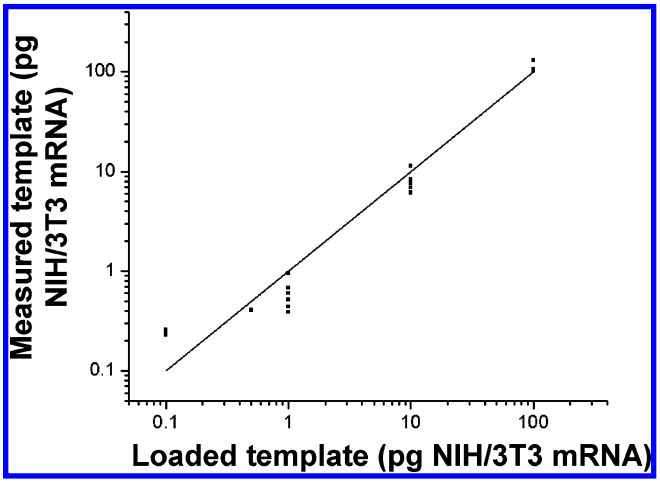

Figure 3. 4plex mRNA isolation calibration and efficiency measurements. A 132-bp portion of GAPDH was amplified and detected. Measured values for 4plex microfluidic standards were extrapolated utilizing an off-chip standard curve (Figure S-2b) generated with known quantities of NIH/3T3 mRNA. The line represents 100% efficiency ($m = 1$).

Microfluidic cDNA Synthesis. Solid-phase cDNA synthesis was implemented on-chip with purified NIH/3T3 mRNA by utilizing the beads as both primers and a support. Gel electrophoresis results from PCR on templates processed microfluidically are shown in Figure 4a. When the reverse transcriptase enzyme was withheld as a negative control, no signal was detected by PCR with 100 pg of NIH/3T3 mRNA or with eight NIH/3T3 cells, demonstrating that DNA contamination within our devices is not an issue. As with the mRNA isolation process, single-cell sensitivity was realized. To calibrate the cDNA synthesis step, we generated a qPCR standard curve fitted to Ct values of known NIH/3T3 mRNA templates subjected to the solid-support first strand cDNA synthesis on the 4plex platform (Figure S-1d). The qPCR standard curve generated from microfluidic samples spans 4 orders of magnitude with a highly reliable correlation coefficient ($R = 0.99$). As with the mRNA isolation procedure, we extrapolated measured values for our known on-chip templates by plotting the Ct values onto an off-chip RT-qPCR standard curve (primers specific to GAPDH, Figure 4b). We obtained an average efficiency of 44% for the coupled mRNA isolation/cDNA synthesis/recovery steps. Because we performed total cDNA synthesis with oligo(dT) primers and then utilized specific primers for the PCR, the on-chip measurements are less efficient than if we were to introduce specific primers into the first strand reaction. The average experimental variability (coefficient of deviation) for the coupled mRNA isolation/cDNA synthesis steps was 19%. This noise can be attributed to the same reasons that were found for the mRNA isolation variability, as well as the aforementioned differences in primers.

Cellular Measurements. Next, we sought to study gene expression in small numbers of NIH/3T3 cells. We first utilized

(25) Pannetier, C.; Delassus, S.; Darche, S.; Saucier, C.; Kourilsky, P. *Nucleic Acids Res.* **1993**, *21*, 577−583.
(26) Rutledge, R. G.; Cote, C. *Nucleic Acids Res.* **2003**, *31*, e93.

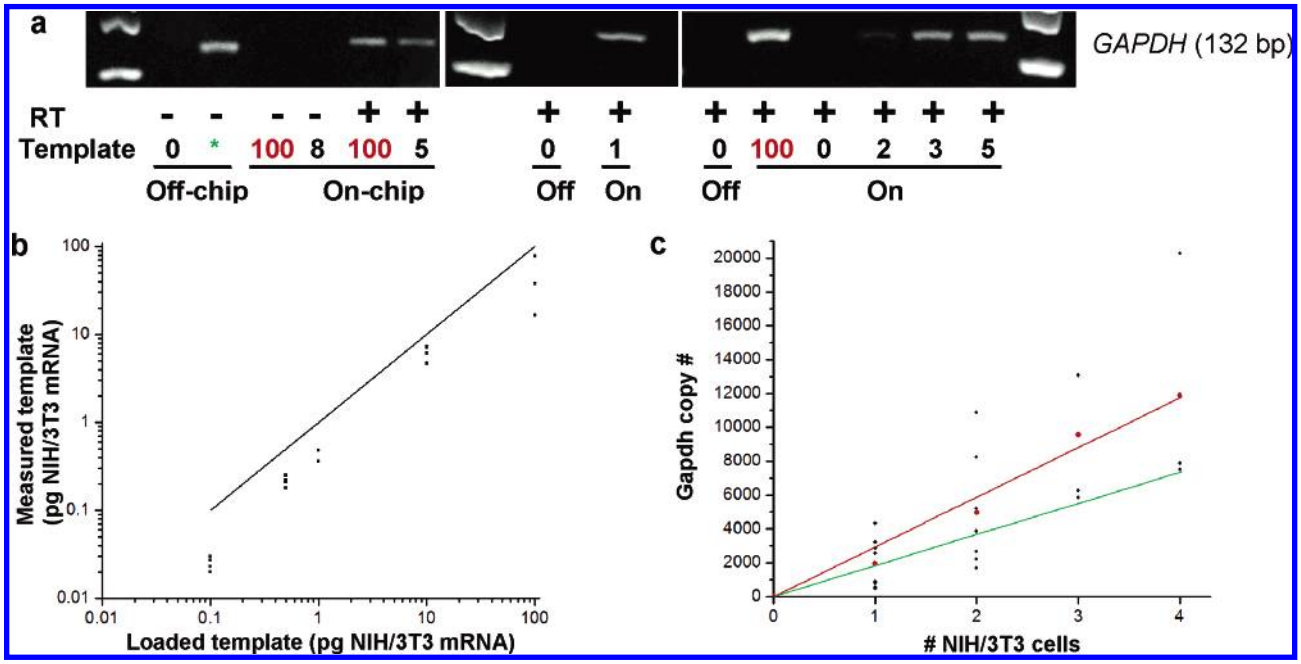

Figure 4. On-chip cDNA synthesis calibration and gene expression measurements in various numbers of cells. (a) Gel electrophoresis results from samples subjected to on-chip cDNA synthesis. Each lane on the 1% agarose gel contains 1 μL of the respective 50-μL PCR reaction. The black and red numbers are number of NIH/3T3 cells and NIH/3T3 mRNA templates in picograms, respectively. The * represents 1 μL of unpurified GAPDH PCR product, utilized as a positive control. (b) 4plex mRNA isolation/cDNA synthesis efficiency data. An off-chip qRT-PCR standard curve (Figure S-2c) was utilized to extrapolate measured values for loaded microfluidic templates (black squares). The line represents 100% efficiency ($m = 1$). (c) Varying levels of GAPDH gene expression in individual cells. The average copy number per NIH/3T3 cell obtained from a bulk experiment was plotted as a green line, $Y = 1836X$. The microfluidic samples were similarly run against a standard curve of known quantities of GAPDH cDNA (Figure S-2a, red) to determine copy number for each sample (black circles). The average copy number for each sample group, adjusted for efficiency of the process, are plotted as red circles, fitted to $Y = 2938X$, $r^2 = 0.98$.

4plex devices to carry out the process of cell capture−cell lysis−mRNA isolation on individual cells ($n = 5$). By comparing the Cts of the NIH/3T3 cellular samples to the off-chip NIH/3T3 mRNA standard curve (Figure S-1c), we obtained a raw estimate of 0.8 pg of mRNA/cell. Upon correcting for the 80% measured efficiency of the process, we estimate an average value of 1 pg mRNA/cell, consistent with published values[27] and slightly better than most commercial kits (Table S-1, Supporting Information).

We then carried out the five-step microfluidic process (cell capture−lysis−mRNA isolation−cDNA synthesis−purification) on various populations of cells, ranging from one to four cells. We subsequently ran off-chip GAPDH cDNA standards (Figure S-1a) to calibrate the GAPDH copy number in each cellular sample (Figure 4c, black circles), as well as to obtain an average copy number for each sample size (Figure 4c, red circles). Based on the raw GAPDH copy number of 1293 copies/cell obtained in the microfluidic cell samples, and after accounting for the 44% efficiency of the method, we estimate an average of 2938 ± 140 GAPDH transcripts per cell. This result is within a factor of 2 of the average of 1837 ± 146 transcripts obtained from bulk measurements (Figure 4c, green line). The bulk average was determined by running mRNA templates isolated from 2500 NIH/3T3 cells against a GAPDH cDNA standard curve (Figure S-1a). For the single-cell samples, the cell-to-cell variation in copy number is rather large, with a coefficient of variation of 0.75 ($n = 8$). This is significantly greater than the random error introduced by processing, which we estimate at 0.19 ($n = 25$). These differences can be most likely attributed to inherent cell-to-cell variation, asynchronization in the cell cycle, and varying metabolic states.

A key feature of the microfluidic process is the ability to generate and recover concentrated mRNA or cDNA products. Because the beads are paramagnetic and therefore can be reconcentrated, they can be flushed out of the device in microliter amounts of buffer without irreversibly diluting the products. The product concentration after mRNA isolation/first strand cDNA synthesis is crucial for the integration of downstream on-chip steps and off-chip validation assays. A byproduct of the column's broad functionality is the versatility gained by the device user in choosing whether to make cDNA after mRNA isolation is complete. Furthermore, the present strategy to build affinity columns shows marked improvement in speed and robustness over the previous implementation[18] (Figure 2d).

The mRNA isolation and cDNA synthesis calibrations show that this technique is reliable for templates that span 4 orders of magnitude in copy number. Notably, we were able to detect the presence of GAPDH and HPRT mRNAs from initial templates of 0.1 and 1 pg of mRNA, respectively, the former being roughly 10−20% of a single cell's mRNA. These results show promise for the detection of low-abundance transcription factors present in single cells. We were also able to show that cell lysis did not have an abnormal effect on subsequent mRNA capture. The mRNA content of single cells was determined by qRT-PCR to fall within 0.5−2.5 pg (Table S-1), values consistent with published values.[27] We also demonstrated the significance of studying single cells as opposed to bulk samples. Figure 4c makes apparent the discrepancy in information attained when studying single cells versus

(27) Alberts, B.; Bray, D.; Lewis, J.; Raff, M.; Roberts, K.; Watson, J. D. *Molecular Biology of the Cell*, 4 ed.; Garland Publishing: New York, 1994.

populations. This approach could have far-reaching implications for gene expression studies in developmental and cancer biology, where individual cells within a population succumb to different fates. Information pertaining to what genes are expressed in low to medium abundance in these individual cells would be impossible to gain from bulk studies that give average values over populations.

The ability to acquire gene expression data from multiple cells, as well as single cells, should not be overlooked. In many cases, such as intercellular signaling studies, it may be of interest to study gene expression in small numbers of cells rather than individual cellular samples. Our technique and device has the dynamic range to support both types of assays. Furthermore, based on the mRNA isolation and cDNA synthesis calibration curves, it is not unreasonable to suspect our processing capabilities to be ≥100 cells/reactor, thus allowing automated preparation of larger samples.

CONCLUSIONS

The device and methodology presented here lay the groundwork for highly parallel economy-of-scale single-cell gene expression analysis. Although we limited the process to four reactions in parallel, the notion of realizing 50−500 reactions on one device is not far in the future. The possible number of samples one can attain with this technology is at least 1 order of magnitude larger than the current state of the art in single-cell gene expression studies. We also demonstrated the method to be a robust one, in that sample concentrations ranging 4 orders of magnitude could be retrieved and detected in a quantitative manner.

ACKNOWLEDGMENT

We thank Kathy Burke for assistance with cell culture and real-time PCR. We also acknowledge Alejandra Torres for assistance with device fabrication and Carl Hansen and Sebastian Maerkl for helpful discussions. This work was supported by a National Research Service Award (T32GM07616) from the National Institute of General Medical Sciences (J.S.M.) and National Institutes of Health (NIH) grant NIH 1RO1 HG002644-01A1.

SUPPORTING INFORMATION AVAILABLE

Additional information as noted in text. This material is available free of charge via the Internet at http://pubs.acs.org.

Received for review October 31, 2005. Accepted February 24, 2006.

AC0519460